REB/Channel Tracking Experiments in Low Pressure Ammonia

D. P. MURPHY, M. RALEIGH, E. LAIKIN,
R. E. PECHACEK, AND J. R. GREIG

Experimental Plasma Physics Branch
Plasma Physics Division

March 26, 1984

DTIC
ELECTE
APR 18 1984
S   D
B

NAVAL RESEARCH LABORATORY
Washington, D.C.

84 04 17 058

REPORT DOCUMENTATION PAGE

1a. REPORT SECURITY CLASSIFICATION	1b. RESTRICTIVE MARKINGS
UNCLASSIFIED	

2a. SECURITY CLASSIFICATION AUTHORITY	3. DISTRIBUTION/AVAILABILITY OF REPORT
2b. DECLASSIFICATION/DOWNGRADING SCHEDULE	Approved for public release; distribution unlimited.

4. PERFORMING ORGANIZATION REPORT NUMBER(S)	5. MONITORING ORGANIZATION REPORT NUMBER(S)
NRL Memorandum Report 5281	

6a. NAME OF PERFORMING ORGANIZATION	6b. OFFICE SYMBOL (If applicable)	7a. NAME OF MONITORING ORGANIZATION
Naval Research Laboratory		Naval Surface Weapons Center

6c. ADDRESS (City, State and ZIP Code)	7b. ADDRESS (City, State and ZIP Code)
Washington, DC 20375	White Oak, Silver Spring, MD 20910 Attn: Dr. C.M. Huddleston (R401)

8a. NAME OF FUNDING/SPONSORING ORGANIZATION	8b. OFFICE SYMBOL (If applicable)	9. PROCUREMENT INSTRUMENT IDENTIFICATION NUMBER
ONR and DARPA		

8c. ADDRESS (City, State and ZIP Code)	10. SOURCE OF FUNDING NOS.			
	PROGRAM ELEMENT NO.	PROJECT NO.	TASK NO.	WORK UNIT NO.
Arlington, VA 22217 Arlington, VA 22209	61153N		RR011-09-41	47-0871

11. TITLE (Include Security Classifications)				
(See page ii)	62707E	1	OR 40 AA	47-0922

12. PERSONAL AUTHOR(S)
D.P. Murphy, M. Raleigh, E. Laikin, R.E. Pechacek, and J.R. Greig

13a. TYPE OF REPORT	13b. TIME COVERED	14. DATE OF REPORT (Yr., Mo., Day)	15. PAGE COUNT
Interim	FROM _____ TO _____	March 26, 1984	33

16. SUPPLEMENTARY NOTATION
This research was supported by the Office of Naval Research and the Defense Advanced Research Projects Agency (DoD), ARPA Order No. 4395 Amendment No. 11, monitored by the Naval Surface Weapons Center under Contract N60921-83-WR-W0114.

17. COSATI CODES			18. SUBJECT TERMS (Continue on reverse if necessary and identify by block number)	
FIELD	GROUP	SUB. GR.	Beam propagation	Channels
			Relativistic electron beams	Tracking

19. ABSTRACT (Continue on reverse if necessary and identify by block number)

→ This document presents

We present the results of an investigation of the interaction between an intense relativistic electron beam (REB) and reduced density channels in ammonia (NH_3) at 40 Torr. The channels were produced by absorption in the ammonia of energy from a pulsed CO_2 laser. Two channel geometries were studied. The first employed an 2.5 cm radius channel with the nominally 1.2 cm radius REB injected coaxially. The second geometry employed an annular channel with its minimum density at 2.3 cm radius and near ambient density on axis. The REB was again injected coaxially. We found that the conductivity induced in the reduced density channel by the REB caused large plasma currents to flow in the channel. The REB current and the plasma current flowed in opposite directions during most of the REB pulse, causing the REB to be expelled/repelled from the channel.

20. DISTRIBUTION/AVAILABILITY OF ABSTRACT	21. ABSTRACT SECURITY CLASSIFICATION	
UNCLASSIFIED/UNLIMITED ☒ SAME AS RPT. ☐ DTIC USERS ☐	UNCLASSIFIED	

22a. NAME OF RESPONSIBLE INDIVIDUAL	22b. TELEPHONE NUMBER (Include Area Code)	22c. OFFICE SYMBOL
D.P. Murphy	(202) 767-2077	Code 4763

DD FORM 1473, 83 APR   EDITION OF 1 JAN 73 IS OBSOLETE.

11. TITLE (Include Security Classification)

REB/CHANNEL TRACKING EXPERIMENTS IN LOW PRESSURE AMMONIA

CONTENTS

DTIC
ELECTE
APR 1 8 1984
B

Accession For

NTIS GRA&I	✔
DTIC TAB	☐
Unannounced	☐
Justification	

By
Distribution/

Availability Codes

| Dist | Avail and/or Special |

A-1

iii

REB/CHANNEL TRACKING EXPERIMENTS IN
LOW PRESSURE AMMONIA

I INTRODUCTION

Particle beams propagating through gaseous atmospheres lose both energy and particles because of scattering on the gas molecules. This process limits the ultimate range of particle beams and the power density achieved at any intermediate range. To extend the range of electron beams in the atmosphere the process of "hole boring" was conceived.[1] Meanwhile, to both guide light ion beams to their targets in Inertial Confinement Fusion (ICF) reactors and to increase the power density on target, reduced density, current-carrying channels produced by laser guided electric discharges have been suggested.[2] In both of these concepts the particle beam propagates in a reduced density channel through the gaseous atmosphere so reducing losses due to scattering.

In a previous experiment[3] we have demonstrated that an intense relativistic electron beam (REB) is guided along a current-carrying, reduced density channel through the atmosphere provided the auxiliary current in the channel is parallel to the REB current (I_B). Then the channel conductivity is large, the plasma return current is always equal and opposite to the beam current and moves with the beam current so that there is no net force on the beam. However the REB is steered along the channel and held together by the magnetic field of the auxiliary current.

At high ambient pressures, i.e., near atmospheric pressure, and for modest REB characteristics, i.e., $\dot{I}_B < 10^{12}$ A/s , the conductivity in the reduced density channel is governed by the inherent conductivity of the hot channel combined with the collisional ionization produced by the beam electrons themselves. However at lower ambient pressures or larger values of $\dot{I}_B$, avalanche ionization can contribute significantly to the channel conductivity. In this manuscript we describe an experiment in which an intense REB has been allowed to propagate in an atomsphere of ammonia at low pressure.[4] Ammonia was chosen for these experiments because of its ability to absorb the energy from a pulsed CO_2 laser which permitted the formation of reduced density channels in an otherwise uniform atmosphere of ammonia.[5,6] At the background pressure of ~ 40 Torr (gas density n_g ~ 1.3×10^{18} cm^{-3}) and with suitable experiment geometry (See Results and Discussion), avalanche

ionization became a major factor in the generation of plasma conductivity. We found that the enhanced conductivity significantly influenced REB propagation.

II APPARATUS

a) The Test Chamber

These propagation experiments were performed in a large test chamber made of fiberglass. The chamber was cylindrical: 1.5 m long and 0.6 m in diameter (figure 1.). The chamber could be lined with brass screen to change from the initial nonconducting wall boundary conditions to conducting wall boundary conditions. One end flange of the chamber was aluminum and was electrically connected through the drift tube to the Pulserad 310[*] electron beam generator. The REB entered the test chamber through a thin titanium foil (~ 0.038 mm) at the center of the aluminum end flange. There were three lucite windows in this flange to permit an xray pinhole camera and two xray PIN diodes to view the interior of the chamber. There were also, windows in the cylindrical body of the fiberglass chamber and in the fiberglass flange at the opposite end of the chamber to accomodate other diagnostics.

The CO_2 laser beam entered the test chamber through a salt (NaCl) window on the end of a 2.5 m long extension tube. This extension tube connected to the test chamber through a fast acting, pneumatically operated, gate valve and was filled with dry nitrogen at the same pressure as the ammonia in the test chamber. The gate valve was opened a few seconds before the firing of the CO_2 laser. This arrangement was necessary to keep the power density of the CO_2 laser pulse, as it came to focus, below the damage limits of the salt window.

b) The REB Generator

The relativistic electron beam (REB) was produced by a modified Pulserad 310 accelerator, consisting of a 10 stage oil-insulated Marx generator driving a 40 ohm oil dielectric Blumlein pulse forming line which was terminated with a cold-cathode field emission diode (figure 2.). Each stage of the Marx generator contained one 0.1 µF at 100 kV capacitor for a total stored Marx energy of 5.0 kJ. Power was switched to the Blumlein pulse forming line through a self-break oil switch and under ideal conditions, the shot-to-shot jitter from trigger-to-Marx to beam firing could be less than ± 20 ns. The diode assembly was a 1.2 cm radius annular carbon cathode (0.63 cm annular width) separated by 1.6 cm from a 0.038 mm thick titanium foil anode.

[*](Physics International Co., San Leandro, Ca)

Typically the electron beam characteristics inside the diode were V = 1.1 MV, I = 24 kA, with a pulse width of 26 ns FWHM. As the anode foil usually ruptured after each shot, an appropriate foil holder was fabricated to allow rapid replacement of the anode. Using several such holders, the time between shots was limited only to that necessary to evacuate the diode to a base pressure of less than 10^{-4} Torr, typically 20 minutes. The accelerator could be fired 15-20 times before a complete cleaning of the diode internal surfaces and a redressing of the cathode was necessary.

The clear aperture of the anode foil was 10.4 cm and the REB current emerging through this aperture had a peak current of approximately 19 kA. The electron beam was transported to the test chamber through a 0.5 m long drift tube containing a conical return current conductor and filled with dry nitrogen at a pressure of approximately 20 Torr. At the far end of the drift tube where it joined the test chamber the return current conductor had converged to a diameter of 2.3 cm and ended in a 2.5 cm thick aluminum block with a 2.3 cm diameter hole in it. The electron beam passing through this hole entered the test chamber through a second titanium foil. The peak electron beam current entering the test chamber was ~ 8 kA and it had a nearly uniform current density profile across the 2.3 cm aperture.[7]

c) The CO_2 Laser

The pulsed CO_2 laser used in these experiments has been described elsewhere,[8] it is a UV preionized TEA laser consisting of an oscillator and three amplifiers. The oscillator has been converted to an off-axis confocal resonator geometry to eliminate unwanted mode structure and the "crescent" shaped output beam was masked at the output of the oscillator to give a nearly uniform, circular laser output beam with diameter 7.5 cm. The pulse delivered to the test chamber contained ~ 300 J of laser energy. The characteristic pulse shape was an initial spike of FWHM ~ 100 ns and a tail of duration ~ 1 μs .

III EXPERIMENTAL PROCEDURE
    a) The Channel

To create reduced density channels in the ammonia gas a 10 m focal length, salt lens focused the CO_2 laser beam through the circular aperture on

the salt window that clipped the laser beam to a 2 cm radius spot at the entrance foil to the test chamber. The distance from the lens to the entrance foil was 4.5 m. The heated gas expanded to form a simple channel of radius ~ 2.5 cm, where the radial profile of the channel was

$$n(r) \sim \frac{n_0}{4} + \frac{3}{4} n_0 \left(\frac{r}{R_{chan}}\right)^4 \quad \text{for } r < R_{chan} . \tag{1}$$

In some of the earlier experiments the spot size at the entrance foil was decreased to 1 cm radius, which formed simple channels of ~ 1.2 cm radius. Annular channels, i.e., channels in which the minimum density occurred off axis and the density on axis remained near ambient density, were created by placing a circular stop at the center of the large circular aperture on the salt lens. The laser spot at the entrance foil was clipped to a 1 cm inner radius and a 2 cm outer radius. The annular channel that was formed had a density minimum at ~ 2.3 cm radius.

In all the channel experiments the ammonia fill pressure in the test chamber was kept constant at 40 Torr. The intensity of the laser beam was approximately constant and because the effects of absorption and focusing were nearly matched, the laser energy deposited in the ammonia gas was fairly uniform at ~ 25 mJ/cm^3 along the length of the channel. This amount of energy (> 0.1 eV/molecule) while several times the thermal energy (~ 0.025 eV/molecule) was negligible compared to the dissociation potential (4.3 eV) and the ionization potential (10.15 eV) of ammonia.[9] At the same time the vibrational-translational relaxation of the excited ammonia molecule is very fast[5], ~ 100 ns at a pressure of 40 Torr. Thus we expected to produce channels in the ammonia that relaxed to pressure equilibrium on hydrodynamic timescales after effectively instantaneous energy deposition and we did not expect the laser to generate any conductivity in the channels.[10] These aspects of the channel history were confirmed using double exposure holographic interferometry[11] and an RF bridge[12] respectively.

The optical layout of the holographic system is shown schematically in figure 3. It examined a cross section of the test chamber 75 cm downstream of the entrance foil. The light source was a Q-switched ruby laser with a pulse duration of ~ 25 ns. For the first several microseconds (< 3 μs) after deposition of the CO_2 laser energy, the density reduction in the channel was

too small to be measured. Thereafter the simple channel was observed to grow steadily reaching pressure equilibrium with the surrounding ambient gas in approximately 50 µs. The channel relaxed without becoming turbulent[13] showing still a factor of two density reduction after 1 ms. In both simple and annular channels the minimum density was approximately one-quarter the ambient density. In addition, for the annular channels the density on axis first rose to approximately twice ambient density at ∼ 50 µs , then settled back close to ambient density by ∼ 100 µs . A typical result for an annular channel is shown in figure 4.

A schematic diagram of the RF bridge is shown in figure 5. Operating at a frequency of 30 MHz, and with a transmission line length of 1.0 m, this system could detect a conductivity as low as ∼ 10^3 s^{-1} in a 4 cm diameter channel. The laser produced conductivity in the channel was always too small to be detected!

b) The Diagnostics

Apart from the channel diagnostics described above, the diagnostic suite for studying REB propagation and REB/channel interaction included a time integrated xray pinhole camera, two xray PIN diodes, three Rogowski coils, and a Faraday cup. There was too little visible emission when the intense REB interacted with ammonia gas at 40 Torr to observe the position of the REB by time integrated visible photography. To test the diagnostic system therefore, the chamber was sometimes filled with dry nitrogen at low pressure, then the position of the REB was observed using time integrated white light photography.

The xray emission from the ammonia gas molecules themselves was also too faint to observe so metal targets in the form of a tungsten wire grid (0.3 mm diameter wire on a 1 cm spacing) and a brass sheet were placed in the test chamber at different distances (z) from the entrance foil. With the targets at z ∼ 0.5 m the xray pinhole camera could see the full diameter of the test chamber with spatial resolution ∼ 1 cm, and the two xray PIN diodes (Quantrad 025-PIN-125) could each see a circle of ∼ 8 cm diameter. The PIN diodes were collimated and shielded inside 13 cm cubes of lead. Also the diode inputs were filtered with metal foils so that they accepted only xrays with energy above 30 keV. The PIN diodes' time resolution was ∼ 2 ns when biased at

5

200 V and they were sensitive enough to detect 0.5 kA of REB in their field of view. The xray pinhole camera used Polaroid film, a 3M Trimax intensifier screen and was shielded from the Pulserad diode and the drift tube by ~ 5 cm of lead.

Rogowski coils were used to measure the net current passing through an aperture. Rogowski coil RC1 was 12 cm in diameter and was mounted at the chamber entrance foil. RC2 and RC3 were 7 cm in diameter and were mounted at z = 1 m on the brass target plate. RC2 was coaxial with the channel and RC1, while RC3 was offset 15 cm. RC3 was used to detect large off-axis excursions of the REB. The time resolution of the Rogowski coils was ~ 3 ns. Both RC2 and RC3 were in the field of view of the xray pinhole camera. When the REB deviated enough to strike one of them, its lead foil shielding glowed brightly in the xray photograph. Such hits sometimes produced unusual signals on a Rogowski coil or even damaged it.

An evacuated Faraday cup[14] collected the charge that passed through its titanium foil window (thickness 0.038 mm), and measured the potential difference generated when that charge flowed back to the generator through a very low inductance coaxial shunt resistor (~ 0.2 x 10^{-3} ohm). The time resolution of the Faraday cup was ~ 1 ns. Periodically we installed the Faraday cup on the Pulserad diode or at the entrance to the test chamber to check the reproducibility of the REB.

IV RESULTS and DISCUSSION
a) Plasma Conductivity

The conductivity, σ , of the gas in the chamber is a function of the electron density and the gas density, $\sigma = \sigma(n_e /n)$. The growth of conductivity was governed by the production rate of electrons generated by the passage of the REB through the gas. Four contributions to the rate equation were direct collisional ionization, avalanche ionization, dissociative attachment and associative recombination,

$$\dot{n}_e = \frac{1}{\chi} \frac{d\epsilon}{dz} \frac{J_B}{-e} + \alpha\, n_e - \eta n n_e - \beta n_e^2 \ . \tag{2}$$

These four terms are implicit and/or explicit functions of the gas density, n,

6

the electron density, n_e, the electric field, E, and the REB current density, J_B. The avalanche ionization coefficient, α, is in particular a very strong function of the density normalized electric field, E/n. Figure 6 is a plot of the density normalized avalanche coefficient, α/n, as a function of E/n for both air and ammonia.[10,15] The avalanche coefficient increases if either the gas density drops, as in a channel, or the electric field increases. Our REB, when injected into the lined test chamber with 40 Torr ammonia present produced an initial normalized electric field of ~ 200 Td. This same REB injected into a reduced density channel would develope a higher density normalized electric field of ~ 800 Td.

Being in the limit where the rise time of the REB was longer than any transit times for electromagnetic waves within the test system, the electric field generated by the REB was $E = L \dot{I}_N$ where I_N is the net current and L is the inductance per unit length seen by the REB. Thus the inductance became a parameter that could alter the electric field. When the test chamber was lined with a conducting screen this lumped circuit inductance was estimated to be that for two concentric coaxial cylinders of radii a = 1.2 cm and b = 30 cm,

$$ L = L_c \simeq \frac{\mu_0}{2\pi} \ln\left(\frac{b}{a}\right) \simeq .5\mu_0 \text{ (H/m)} . \tag{3} $$

The test chamber sat in a metal walled room of 3 x 3 m cross section. When the screen liner was removed from the test chamber the outer conducting boundary radius, b, defaulted to that of the metal experimental room, b ~ 150 cm. The estimated lumped circuit inductance for the nonconducting test chamber was L_{nc},

$$ L = L_{nc} \simeq \frac{\mu_0}{2\pi} \ln\left(\frac{150}{1.2}\right) \simeq .8\mu_0 \text{ (H/m)} . \tag{4} $$

Since $L_{nc} > L_c$ the density normalized electric field, E/n, was larger when the conducting liner was removed from the test chamber.

The external "knobs" that were turned in this experiment were the gas density and the boundary conditions. Both these parameters worked through the rate equaion to adjust the conductivity generated by the passage of the REB.

7

b) Plasma Current

The plasma current is the difference between the net current and the REB current: $I_p(t) = I_N(t) - I_B(t)$. In figure 7 we see that the plasma current was negative, i.e., it flowed back toward the entrance foil during most of the REB pulse. It was during this time, when the REB current and the plasma current were in opposite directions, that the instabilities affecting propagation arose. In general, when the returning plasma current was larger, the net current was smaller and the instabilities were stronger and more destructive. Since the Faraday cup intercepted the REB it was only used periodically to insure the reproducibility of the REB. However, we did monitor the net current, and thus the plasma current, at the entrance foil with Rogowski coil RC1 on every shot.

We found we can describe the behavior of the REB in the test chamber in terms of a parameter f^*, where

$$f^* = 1 - \frac{(I_N)_{max}}{(I_B)_{max}} < \left\{ -1 \frac{\left|(I_p(t)\right|}{(I_B(t))} \right\}_{max} \text{ for } t < 20 \text{ ns.} \qquad (5)$$

Note that the peaks of the net current pulse and of the typical REB current pulse were not simultaneous, but these peak values were quickly obtainable from the photographic data. The observed behavior of the REB for different values of f^* is listed in Table 1.

f^*	Behavior
~ 0.0	REB goes straight - slight kinking visible
~ 0.3	Moderate hosing evident
~ 0.5	Violent hosing evident
~ 0.7	REB dispersed

Table 1

A stability analysis[16] of a flat current profile REB injected into a collisional plasma showed a marked dependence for many transverse oscillations on the ratio of the plasma current to the beam current. The "hose" mode was absolutely growing whenever the plasma current was negative (figure 7.), but many other fast growing modes were triggered when the returning plasma current reached 50% of the REB current. It is difficult to make quantitative comparisons of instability growth with theory because theory is based on small

8

amplitude linear approximations whereas all observations were of large amplitude perturbations of the REB. We did find throughout this study that whenever $f^* > 0.5$ the beam oscillations became particularly violent.

c) Propagation in Dry Nitrogen

To test the diagnostic suite, propagation experiments were first performed in dry nitrogen so that we could have time integrated white light photographs to correlate with the other diagnostics. When the REB entered the gas filled test chamber it expanded to a radius somewhat larger than the 1.2 cm radius of the entrance aperture because it had been heated by its passage through the entrance foil($kT_{\perp} < 1 \times 10^5$ eV per foil). At a fill pressure of 0.5 Torr N_2 the REB propagated the length of the test chamber with only slight kinking evident ($f^* \approx 0$). There was little or no dependence on the boundary conditions, i.e., on the presence or absence of a conducting liner inside the fiberglass test chamber.

When the fill pressure was raised to 40 Torr N_2 the boundary conditions strongly influenced the REB trajectory. With the brass liner in place the REB exhibited moderate hosing action. Its position deviated by < 15 cm from the chamber axis by the time it had propagated to $z = 1$ m. The measured value of f^* was ≈ 0.3. With nonconducting boundary conditions, f^* rose to ≈ 0.5 and the REB frequently struck the chamber walls ($r \approx 30$ cm) by $z = 1$ m. The increase in f^* indicated an increased plasma current generated along the REB trajectory. Since neither the gas density nor the REB itself had been altered it appeared that the changed inductance had altered the electric field and with it the plasma conductivity through the electron rate equation.

d) Propagation in Ammonia Without Channels

The fill pressure for the ammonia studies was also 40 Torr. We measured an f^* of < 0.3 with the conducting liner in place (figure 8a.) and f^* rose to ≈ 0.5 when the liner was removed (figure 8c.). The REB was moderately unstable at $f^* < 0.3$ and violently unstable at $f^* \approx 0.5$. The terms in the rate equation have very similar values for air and ammonia so the similarity in behavior of the REB and in f^* values was not unexpected.

9

e) REB/Channel Interaction in Ammonia

When the REB with a nominal radius of 1.2 cm was injected into a simple channel of radius ~ 2.5 cm with the test chamber lined by the conducting screen we measured only small decreases in the net current compared to the case without the channel ($f^* > 0.3$) (figure 8b). The REB was ejected from the channel but was not measurably more unstable than the case without the channel. However when we decreased the radius of the channel from ~ 2.5 cm to ~ 1.2 cm, i.e., to a radius more comparable to that of the REB, the REB was symmetrically ejected from the channel region. Xray photographs of a tungsten wire grid at z = 0.2 m showed faint annular patterns. The small simple channel in the lined test chamber had not significantly altered the net current but it had more effectively constrained the plasma current to the axis, which caused the symmetric ejection of the REB.

The effect of the ~ 2.5 cm radius simple channel on the REB in an unlined test chamber was quite dramatic. The measured f^* jumped to $f^* \approx 0.7$ (figure 8d) and the REB disrupted so violently that no trace of it could be detected on targets as close as z = 0.5 m. The combination of the reduced density in the channel and the inductive enhancement of the electric field generated by the REB altered the rate equation terms sufficiently to make avalanche ionization completely dominant.

The results of all tests with simple channels in a 40 Torr ammonia background showed that the REB was not attracted to nor guided by the reduced density channel. Preferential ionization within the channel appeared to concentrate the plasma current which then ejected the REB. Reduced density within the channel, not the gas temperature there, was the factor leading to the preferential ionization within the channel. Indeed, for very short delay times after the laser pulse, when the gas was hottest but still at ambient density, the "channel" did not noticibly affect the REB.

The simple channel results led us to attempt trapping the REB inside the core of an annular channel in the unlined test chamber. Computer models[17] had predicted that such a geometry would be stabilizing if the return plasma current could be held outside the REB. The annular channel had a density minimum of 25% ambient density at a radius of ~ 2.3 cm and ambient density on axis. We varied the injection timing from 20 μs to 20 ms after the laser pulse and on occasion pushed the laser even harder to make a deeper channel

but the REB was always quickly ejected from the channel region and then hosed violently inside the test chamber.

Subsequently we made a holographic study of the region of the channel next to the entrance foil. In contrast to the smooth symmetric annular channels we had seen at z = .75 m we found that the annular structure was disrupted near the foil. Our previous measurements of the laser energy deposition in the ammonia gas indicated that about half the available energy would actually be absorbed by the gas. We found that a portion of the remainder was being deposited in a surface plasma generated on the entrance foil. A high pressure bubble formed and expanded outward. This did not significantly alter the shape of a simple channel, but the annular channel was no longer annular. The REB had to traverse this transition region before it could possibly enter the core of the annulus. On the rare occasions that the downstream Rogowski coil, RC2, gave a signal, it was impossible to determine if part of the REB had tracked down the channel or if the REB had simply "hosed" across the coil from outside the channel.

The high pressure disturbance expanded outward ~ 15 cm in the first 100 μs . We installed an aperture plate at the entrance foil with a 15 cm long by 1.7 cm inner diameter thin-walled copper tube protruding out into the core of the annular channel. Unfortunately half the REB was lost at the reduced aperture and, as the REB tried to expand in the ambient gas inside the tube, more of the REB was lost to the tube walls. Less than 1 kA of the REB pulse emerged from the tube into the channel core. Such a low current pulse could not generate enough plasma current to derive any benefit from the annular channel. This low current REB propagated straight ahead whether or not a channel was present.

f) Computer Model

The rate equation for the production of electrons, Eq. (2), was the starting point for the computer model. The first term is the collisional ionization rate,

$$\frac{1}{\chi} \frac{d\epsilon}{dz} \frac{J_B}{e} \simeq 5.3 \times 10^{-9} \times n \times J_B \quad (cm^{-3} \ sec^{-1}) \ , \tag{6}$$

11

where we have substituted

$$\chi \simeq 26.5 \text{ eV per ion/electron pair for ammonia} ,$$

and

$$\frac{d\varepsilon}{dz} \simeq n \times 6.8 \times 10^{-17} \text{ (eV/cm)} \text{ for ammonia} .$$

The second term includes the avalanche ionization coefficient,

$$\alpha = 3.29 \times n \times \sqrt{(E/n)} \times \exp(-2.2 \times 10^{-17}/(E/n)) \text{ (sec}^{-1}) . \qquad (7)$$

The third term includes the attachment coefficient,

$$\eta \simeq 8 \times 10^{-12} \text{ (cm}^3 \text{ sec}^{-1}) . \qquad (8)$$

The fourth term includes the recombination coefficient,

$$\beta \simeq 1 \times 10^{-7} \text{ (cm}^3 \text{ sec}^{-1}) . \qquad (9)$$

CGS units were used in all these equations.

The rate equation was supplimented with equations from a lumped parameter circuit model of the REB/plasma interaction,

$$I_N(t) = I_B(t) + I_p(t) , \qquad (10)$$

where I_N was the net current, I_B was the REB current, and I_p was the total plasma current generated in both the background gas and in any channel that was present. The plasma current was negative during most of the REB pulse. Ohm's law related the plasma current to the electric field,

$$I_p = A \sigma E , \qquad (11)$$

where A was the area of the plasma, and E was the electric field present, which was assumed to be uniform across the plasma in this simple model. The conductivity, $\sigma(n_e/n)$, was calculated for both channel and background gas regions. Faraday's law related the electric field to the time derivative of the current,

12

$$E = L \, \dot{I}_N = L(\dot{I}_B + \dot{I}_p) \, , \tag{12}$$

where L was the lumped curcuit inductance that was derived earlier appropriate to the boundary conditions of the particular test. This last equation was rewritten as

$$E = L \, \dot{I}_B + L A \sigma \dot{E} + L A \dot{\sigma} E \, , \tag{13}$$

$$\text{or} \qquad \dot{E} = \frac{(E - L\dot{I}_B)}{L A \sigma} - \frac{\dot{\sigma}}{\sigma} E \, , \tag{14}$$

so that we had rate equations for both the electron density and the electric field. Starting from an initial set of conditions the equations were stepped iteratively in time to predict each of the quantities of interest. The REB current was assumed to have a uniform current density and to be a half-sinusoid of 35 ns duration, which peaked at 8 kA. The boundary conditions had a conducting wall placed at a radius of 30 cm (liner installed) or at 150 cm (liner removed). The background gas density was that appropriate to the fill pressure of 40 Torr. The channel gas density was set to one-fourth the fill density and the channel was flat bottomed. The REB radius and the channel radius were independently adjustable. The channel radius could be set to zero to simulate the shots with no channels.

The results of the calculation for four combinations of experimental conditions are listed in Table 2. The combinations were:

    a) liner installed - no channel

    b) liner installed - simple channel present

    c) liner removed - no channel

    d) liner removed - simple channel present.

Table 2

	R_{beam}	R_{chan}	R_{wall}	f^*_{calc}	f^*_{meas}
a)	2 cm	0 cm	30 cm	.30	~ .3
b)	2	2	30	.58	~ .3
b)*	6	2	30	.33	~ .3
c)	2	0	150	.47	~ .5
d)	2	2	150	.71	~ .7

The model predicted values of f^* very close to those actually measured in the experiment for sets of parameters that closely matched the true experimental conditions. The one exception was case b). In case b)* the REB radius was inflated to 6 cm to match the calculated f^* value to the measured f^*. In the model the effect of increasing the beam radius was to decrease both the collisional and avalanche ionization terms in the rate equation for the channel, thus lowering the overall conductivity. In the test chamber we found in case b) that the REB quickly wandered out of the channel, thereby reducing the electron production rate in the channel. Our simple model assumed a uniform REB current density and no displacement between the REB and the channel. But note the REB current density on axis for a 6 cm radius uniform beam is the same as that for a Bennett profile REB with a radius of 2 cm and displaced by only 1.4 Bennett radii off axis. We typically saw displacements of the REB of ~ 10 cm by the time it reached the target at z = 1 m, so the artifice of inflating the REB radius is not so unreasonable. A calculation with the displaced REB would more closely match the experimental conditions but was beyond the scope of this simple model.

The effect of changing the experimental conditions was to alter the values and relative importance of the terms in the rate equations. For example, in case d), the avalanche ionization rate in the channel was increased by approximately two orders of magnitude over case a) and dominated the other terms in the electron rate equation. The model predicted a large increase in the channel conductivity and a very localized plasma return current, exactly as observed in the experiment.

V   CONCLUSION

We have injected an intense REB into a test chamber filled with 40 Torr ammonia gas and observed the effect of boundary conditions and reduced density channels on the propagation of the REB. We have also shown that a simple computer model of the interaction accurately forecasts the most important macroscopic parameters of the interaction. The passage of the REB through the gas generated conductivity. The conductivity was governed by the rate equation for electron production. Under appropriate conditions, i.e., an enhanced E field due to a remote conducting boundary and the presence of a reduced density channel, the avalanche ionization term became dominant and the conductivity within the channel increased dramatically. This led to a large plasma return current (f^* $\approx$ 0.7) localized to the density channel and the REB was completely disrupted. When the experimental conditions were adjusted so the avalanche term was less dominant (f^* $\approx$ 0.3 to 0.5) the REB was again ejected from the channel and was hose unstable but did not break apart. At no time did the simple density channels attract or guide the REB; their effect was always disruptive. Certain computer codes have predicted that if a high conductivity region could be localized in an annular shape around a coaxially injected REB it would have a stabilizing effect on the REB. We were not able to confirm this prediction experimentally.

VI   ACKNOWLEDGMENTS

VII REFERENCES

1. Fact Sheet, DoD Particle Beam (PB) Technology Program, February 1983.

2. G. Yonas, Proc 3rd International Topical Conference on High Power Electron and Ion Beam Research and Technology, Novosibirsk, USSR, July 1979.

3. D.P. Murphy, M. Raleigh, E. Laikin, J.R. Greig and R.E. Pechacek, Proc 9th Symposium on Engineering Problems in Fusion Research, Chicago, Ill October 1981. (IEEE Publication # 81CH1715-2 NPS Vol II p1548).

4. D.P. Murphy, M. Raleigh, R.E. Pechacek and J.R. Greig, Proc 5th International Conf on High Power Particle Beams, San Francisco, Ca, September 1983.

5. J.N. Olsen, J Appl Phys, $\underline{52}$, 3279 (1981).

6. K.A. Saum and D.W. Koopman, Phys Fluids, $\underline{15}$, 2077 (1972).

7. Subsequently we have found that the centroid of the beam current is not always on the axis of symmetry of the drift tube and the direction of propagation is not necessarily axial, see M. Raleigh, et. al., NRL Memorandum Report in press.

8. R.E. Pechacek, J.R. Greig, M. Raleigh and S.R. Rod, NRL Memorandum Report 3602 (1977).

9. G. Herzberg, Electronic Structure of Polyatomic Molecules, D. van Nostrand Co., New York (1966), p609.

10. A.W. Ali, NRL Memorandum Report 5150 (1983).

11. F.C. Jahoda in Modern Optical Methods in Gas Dynamic Research, edited by D.S. Dosanjh, Plenum press, New York (1971), p137 (see also F.C. Jahoda and R.E. Siemon, Los Alamos Report, LA5058-MS (1972)).

12. R.E. Pechacek, et.al., NRL Memorandum Report in press.

13. J.M. Picone and J.P. Boris, Phys Fluids, $\underline{26}$, 365 (1983) (see also. J.R. Greig, et. al., NRL Memorandum Report in press.)

14. The basic design for the Faraday cup was given to us by Dr. R.K. Parker of NRL.

15. A.W. Ali, NRL Memorandum Report 4794 (1982).

16. H.S. Uhm and M. Lampe, NRL Memorandum Report 4767 (1982).

17. R.F. Hubbard, R.F. Fernsler, S.P. Slinker, A.W. Ali, M. Lampe, G. Joyce and J.M. Picone, Proc 5th International Conf on High Power Particle Beams, San Francisco, Ca, September 1983.
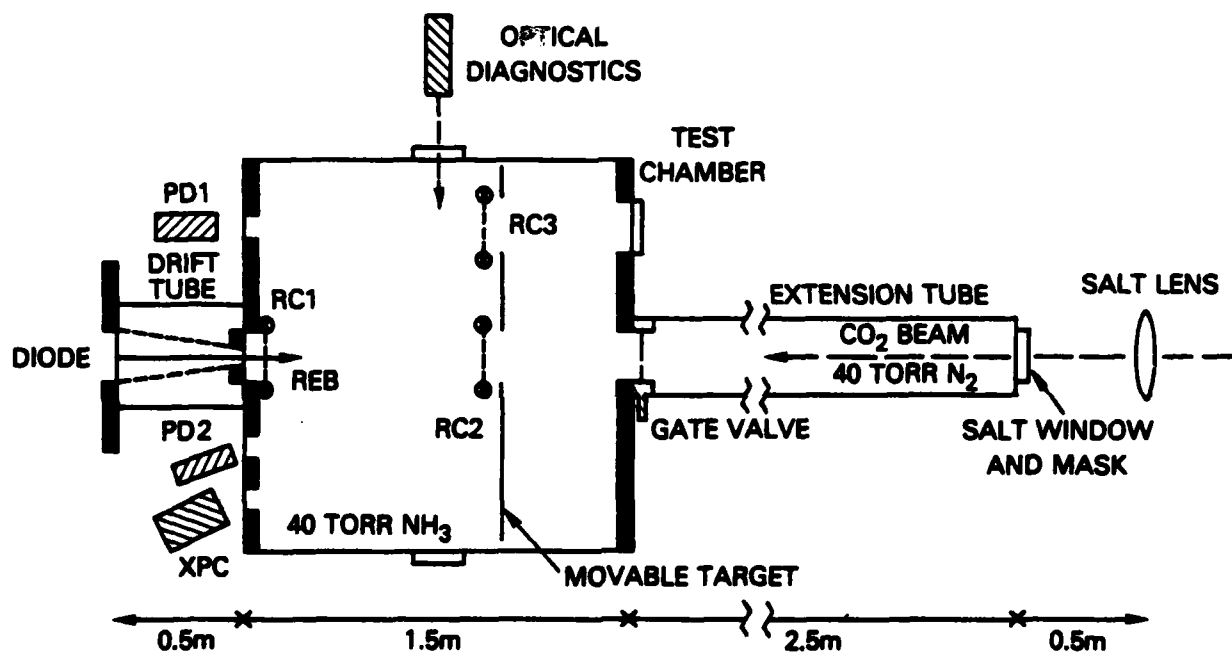
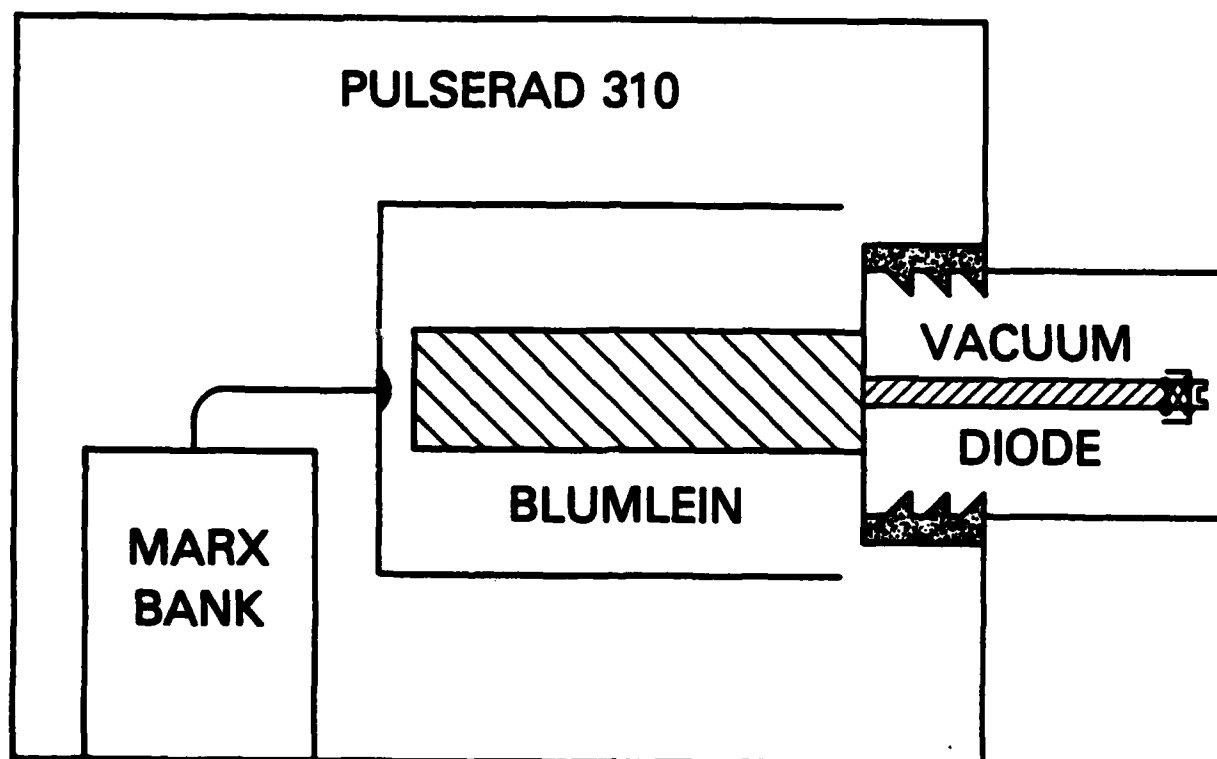Figure 1. Schematic diagram of the test chamber.

17

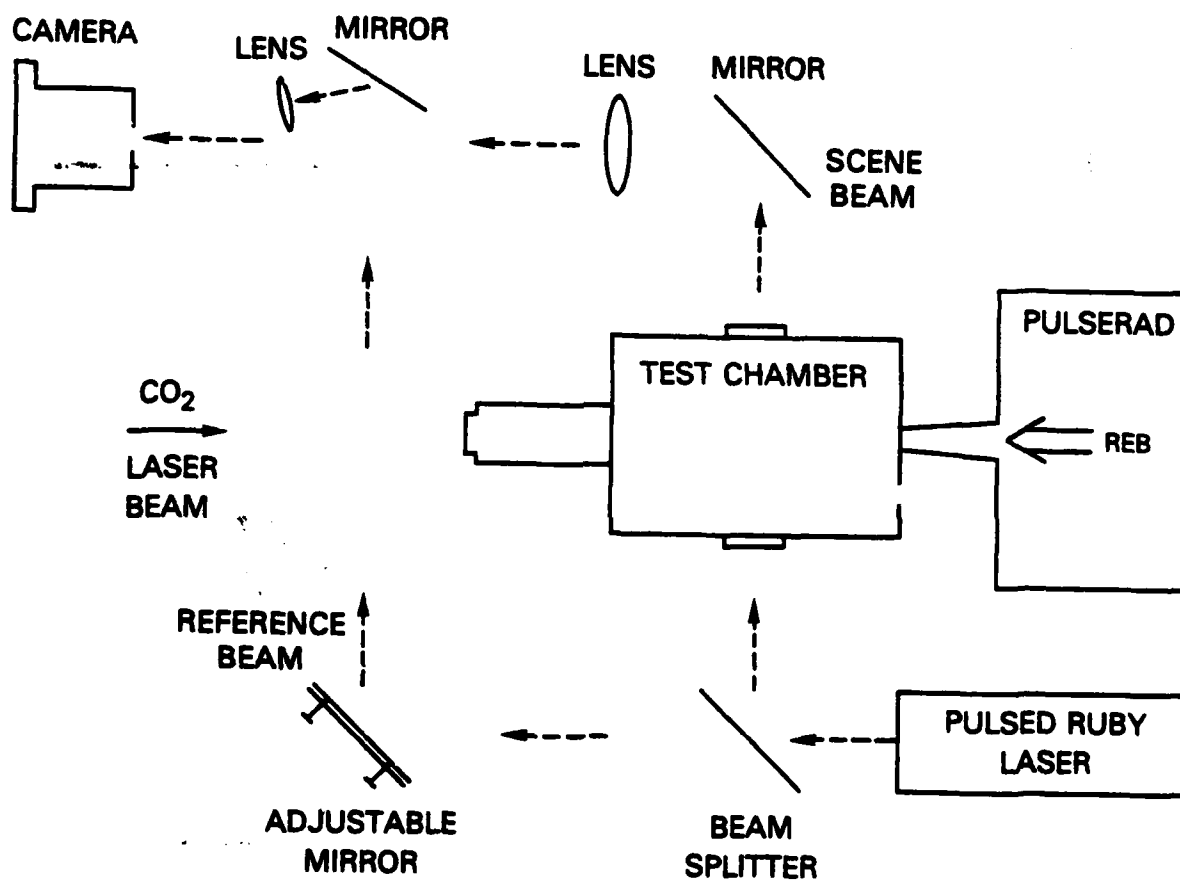Figure 2. Schematic diagram of the Pulserad 310 REB generator.

Figure 3. Schematic diagram of the double-exposure, holographic interferometer.
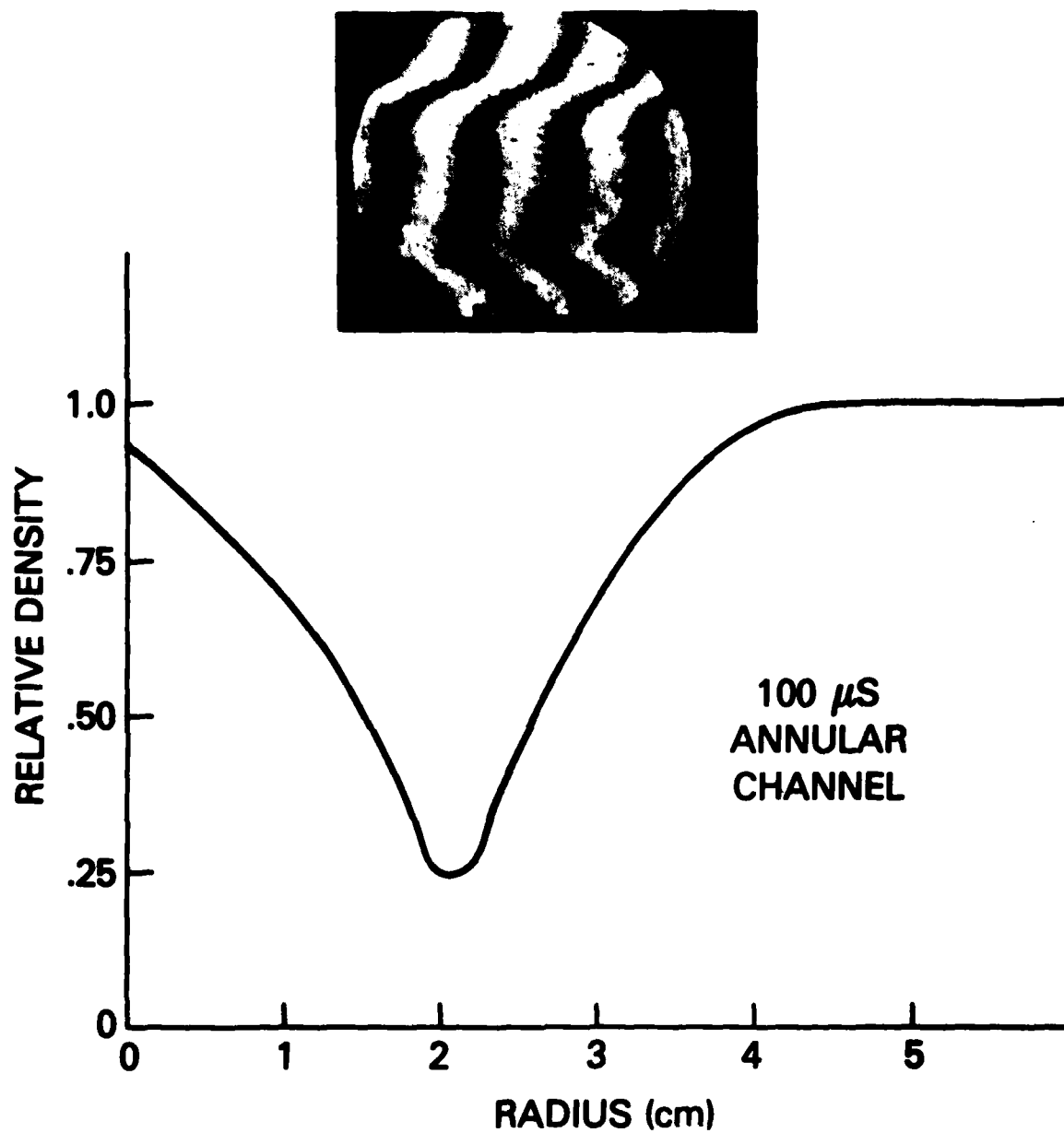
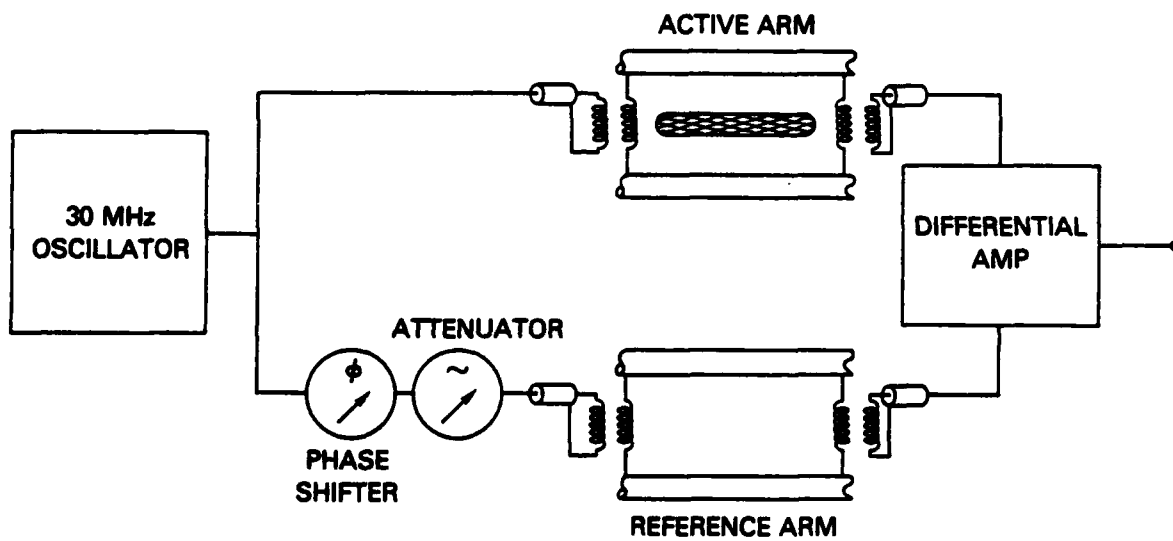Figure 4. Interferometric hologram and its Abel inverted density profile for an annular channel.

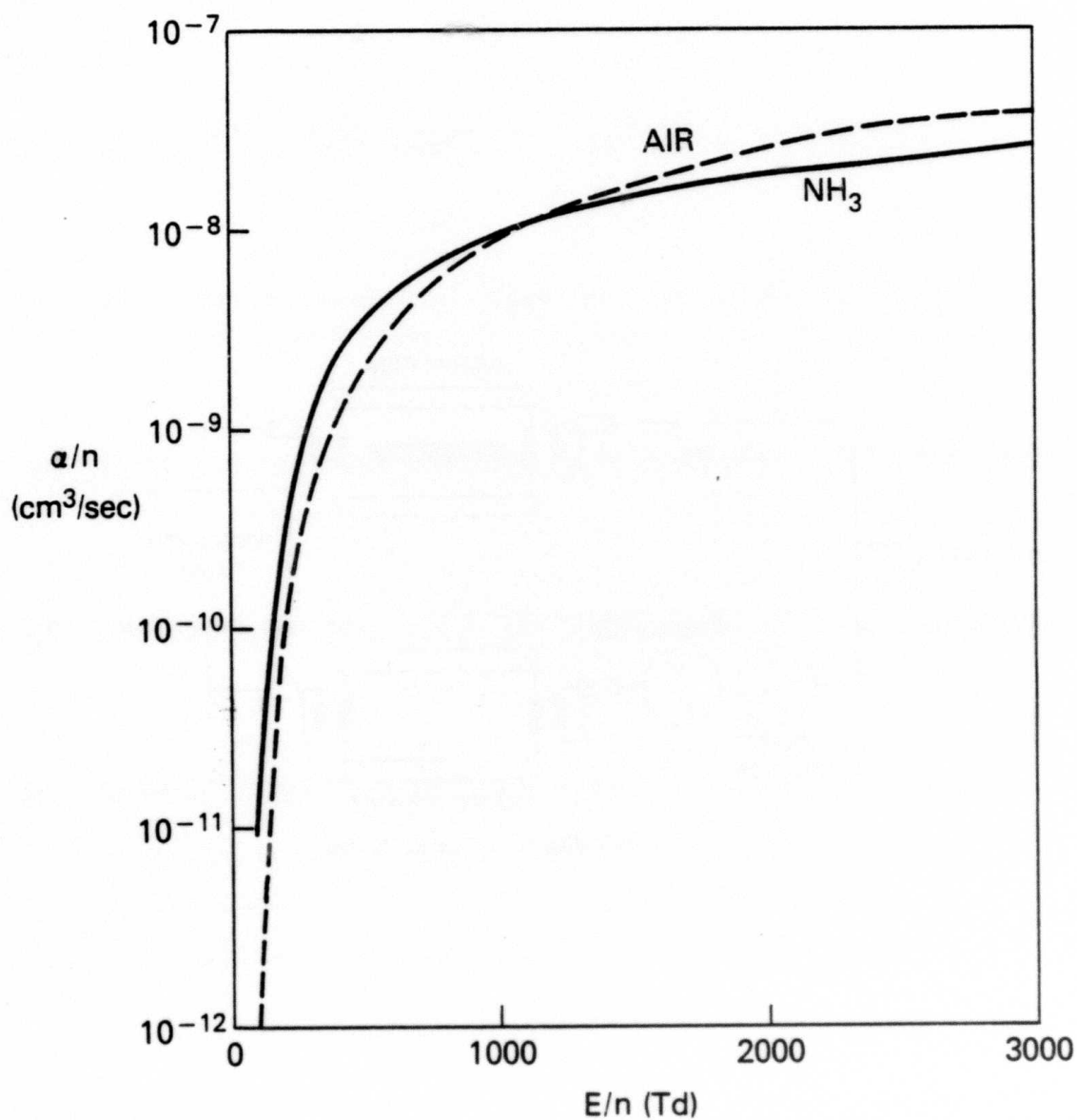Figure 5. Schematic diagram of the RF bridge.

Figure 6. The ionization rate as a function of the electric field, both normalized to the gas density, for air and ammonia (NH_3). (1 Td = 1×10^{-17} V cm^2). The rate for ammonia is based on a formula developed by R. Fernsler.

22

FARADAY
CUP SIGNAL

ROGOWSKI
COIL SIGNAL

$$I_p(t) = I_N(t) - I_B(t)$$

a) REB CURRENT I_B (kA)

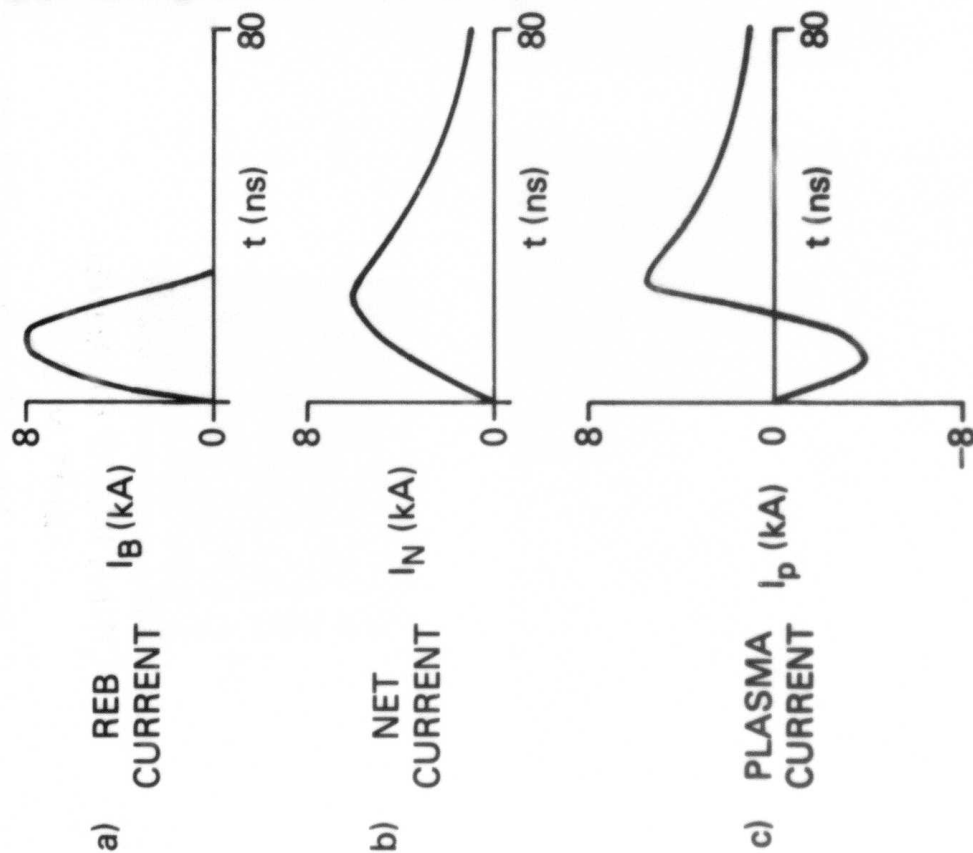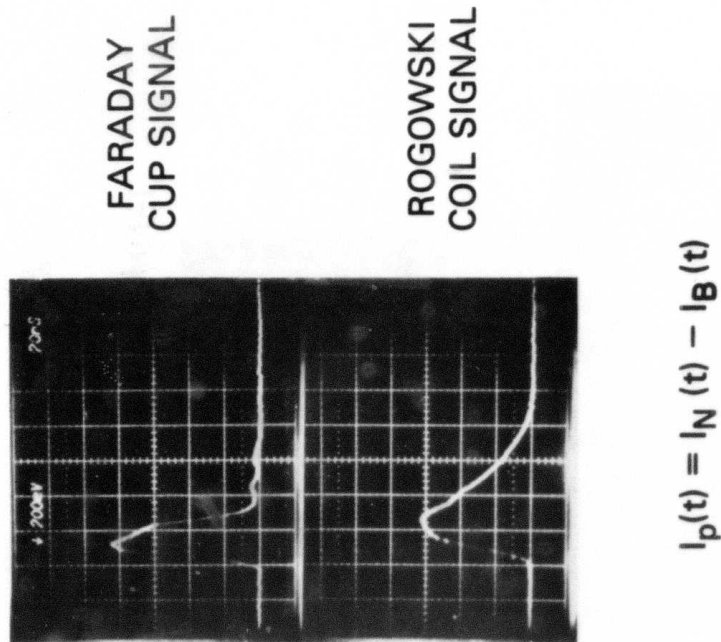b) NET CURRENT I_N (kA)

c) PLASMA CURRENT I_p (kA)

t (ns)

Figure 7. a) The true REB current as measured by the Faraday cup. b) The net current as measured by a Rogowski coil. c) The true plasma current.

23

XPC

XPC

PD1

PD2

PD1

PD2

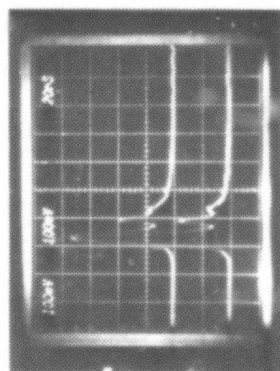LINER IN/NO CHANNEL
(a) f* ∼ .3
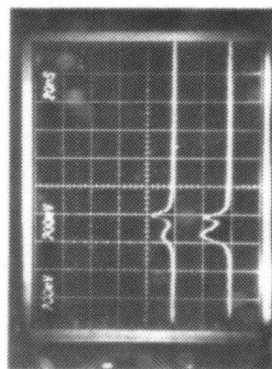
LINER IN/WITH CHANNEL
(b) f* ∼ .3

Figure 8. Xray pinhole photographs and PIN diode signals for the cases with a) Liner in/no channel,
b) Liner in/with channel, c) Liner out/no channel, d) Liner out/with channel.

24

XPC

XPC

LINER OUT/NO CHANNEL
(c) f* ~ .5

PD1
PD2
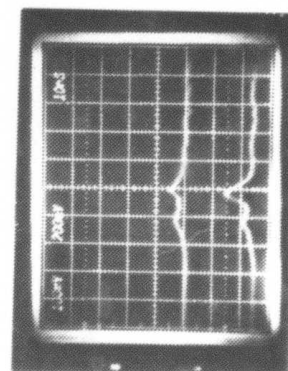
PD1
PD2

LINER OUT/WITH CHANNEL
(d) f* ~ .7

Figure 8. (Continued) Xray pinhole photographs and PIN diode signals for the cases with a) Liner in/no channel, b) Liner in/with channel, c) Liner out/no channel, d) Liner out/with channel.
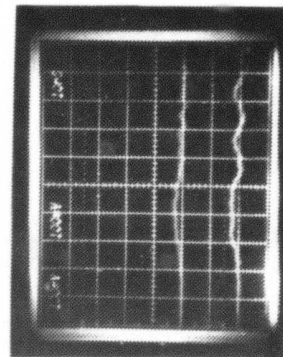
25

DISTRIBUTION LIST

1. Dept. of the Navy
   Chief of Naval Operations
   Washington, D.C. 20350
       ATTN: Dr. C. F. Sharn (op 987)

2. Commander
   Naval Sea Systems Command
   Department of the Navy
   Washington, DC 20363
       ATTN: NAVSEA/PMS 405 (Capt R.L. Topping)

3. Air Force Weapons Laboratory (NTYP)
   Kirtland Air Force Base
   Albuquerque, New Mexico 87117
       ATTN: Maj. James Head
              Dr. David Straw

4. U.S. Army Ballistics Research Laboratory
   Aberdeen Proving Ground, Maryland 21005
       ATTN: Dr. D. Eccleshall (DRDAR-BLB)

5. Ballistic Missile Defense Advanced Technology Center
   P. O. Box 1500
   Huntsville, Alabama 35807
       ATTN: Dr. L. Harvard (BMDSATC-1)

6. B-K Dynamics Inc.
   15825 Shady Grove Road
   Rockville, Maryland 20850
       ATTN: Dr. R. Linz

7. Lawrence Livermore Laboratory
   University of California
   Livermore, California 94550
       ATTN: Dr. R. J. Briggs
             Dr. T. Fessenden
             Dr. W. Barletta
             Dr. D. Prono

8. Mission Research Corporation
   735 State Street
   Santa Barbara, California 93102
       ATTN: Dr. C. Longmire
             Dr. N. Carron

9. Pulse Sciences Inc.
    14796 Wicks Blvd.
    San Leandro, CA 94577
            ATTN: Dr. S. Putnam

10. Science Applications, Inc.
    Security Office
    5 Palo Alto Square, Suite 200
    Palo Alto, California 94304
            ATTN: Dr. R. R. Johnston
                   Dr. Leon Feinstein

11. Naval Surface Weapons Center
    White Oak Laboratory
    Silver Spring, Maryland 20910
            ATTN: Mr. R. J. Biegalski
                   Dr. R. Cawley
                   Dr. J. W. Forbes
                   Dr. C. M. Huddleston
                   Dr. H. S. Uhm
                   Dr. R. B. Fiorito

12. C. S. Draper Laboratories
    555 Technology Square
    Cambridge, Massachusetts 02139
            ATTN: Mr. E. Olsson

13. Physical Dynamics, Inc.
    P. O. Box 1883
    LaJolla, California 92038
            ATTN: Dr. K. Brueckner

14. Office of Naval Research
    Department of the Navy
    Arlington, Virginia 22217
            ATTN: Dr. W. J. Condell (Code 421)

15. Avco Everett Research Laboratory
    2385 Revere Beach Pkwy.
    Everett, Massachusetts 02149
            ATTN: Dr. R. Patrick
                   Dr. Dennis Reilly

16. Defense Technical Information Center
    Cameron Station
    5010 Duke Street
    Alexandria, Virginia 22314 (2 copies)

17. Naval Research Laboratory
    Washington, D. C. 20375
        ATTN: T. Coffey - Code 1001
                M. Lampe - Code 4792
                M. Friedman - Code 4700.1
                J. R. Greig - Code 4763 (50 copies)
                I. M. Vitkovitsky - Code 4701
                W. R. Ellis - Code 4000
                S. Ossakow, Supt. - 4700 (20 copies)
                Library - Code 2628 (22 copies)
                A. Ali - Code 4700.1T
                D. Book - Code 4040
                J. Boris - Code 4040
                S. Kainer - Code 4790
                A. Robson - Code 4760
                M. Picone - Code 4040
                M. Raleigh - Code 4763
                R. Pechacek - Code 4763
                J. D. Sethian - Code 4762
                K. A. Gerber - Code 4762
                G. Joyce - Code 4790
                D. Colombant - Code 4790
                B. Hui - Code 4790

18. Defense Advanced Research Projects Agency
    1400 Wilson Blvd.
    Arlington, Virginia 22209
        ATTN: Dr. J. Mangano
               Lt. Col. R.L. Gullickson

19. JAYCOR
    205 S. Whiting St.
    Alexandria, Virginia 22304
        ATTN: Dr. R. Hubbard

20. Mission Research Corp.
    1720 Randolph Road, S. E.
    Albuquerque, New Mexico 87106
        ATTN: Dr. Brendan Godfrey

21. Princeton University
    Plasma Physics Laboratory
    Princeton, New Jersey 08540
        ATTN: Dr. F. Perkins, Jr.

22. McDonnell Douglas Research Laboratories
    Dept. 223, Bldg. 33, Level 45
    Box 516
    St. Louis, Missouri 63166
        ATTN: Dr. Michael Greenspan
               Dr. J. C. Leader

23. Cornell University
    Ithaca, New York 14853
        ATTN: Prof. David Hammer

24. Sandia Laboratories
    Albuquerque, New Mexico 87185
        ATTN: Dr. Bruce Miller, 4255
               Dr. Carl Ekdahl
               Dr. M. Mazarakis

25. Naval Air Systems Command
    Washington, D. C. 20361
        ATTN: Dr. J. Reif, Code AIR-350F

26. Beers Associates, Inc.
    P. O. Box 2549
    Reston, Virginia 22090
        ATTN: Dr. Douglas Strickland

27. U. S. Department of Energy
    Washington, D. C. 20545
        Office of Fusion Energy, ATTN: Dr. W. F. Dove
        Office of Inertial Fusion, ATTN: Dr. Richard L. Schriever
        Office of High Energy and Nuclear Physics-ER20:GTN,
            ATTN: Dr. T. Godlove

28. AFOSR/NP
    Bolling Air Force Base, Bldg. 410
    Washington, D. C. 20331
        ATTN: Capt. H. Pugh

29. Foreign Technology Division
    Wright Patterson AFB, OH 45433
        ATTN: Mr. C. J. Butler/TQTD

30. Aerospace Corp.
    P. O. Box 92957
    Los Angeles, CA 90009
        ATTN: Dr. A. Christiansen A6/2407

31. SRI International
    333 Ravenswood Avenue
    Menlo Park, CA 94025
        ATTN: Dr. D. Eckstrom

32. Los Alamos National Laboratory
    Los Alamos, NM. 87545
        ATTN: Dr. T. P. Starke, M-2

33. G T Devices
    5705 General Washington Drive
    Alexandria, VA 22312
        ATTN: Dr. D. A. Tidman
               Dr. S. A. Goldstein